Design and Measurement Dug-Hex Antenna for V2V Communications

Ikram Troudi[1,*], Chokri Baccouch[2], Mohamed-Ali Boujemaa[3] and Belgacem Chibani[1]

[1]*MACS Laboratory: Modeling, Analysis and Control of Systems, LR16ES22, National Engineering School of Gabes, University of Gabes, Tunisia*

[2]*Sys'Com, ENIT, Tunis, Tunisia*

[3]*Innov'COM Research Laboratory, Sup'Com, University of Carthage, Tunis, Tunisia*

Abstract

The present study investigates the design, fabrication, and validation of an FSS reflector-based antenna for enhancing the efficiency of Vehicle-to-Vehicle (V2V) communication in Internet of Things (IoT) applications. The proposed design integrates a compact antenna of size 24 mm × 30 mm × 1.6 mm with an FSS unit cell of 10 mm × 10 mm × 1.6 mm. The combination results in a significant improvement in gain, increasing from 1.46 dB to 6.42 dB at 5.9 GHz, along with a broader bandwidth of 738.86 MHz. The research highlights the effectiveness of FSS technology in amplifying antenna gain and bandwidth, demonstrating its potential to enhance V2V communication systems within IoT environments. A prototype of the proposed design is fabricated, and the measurement results validate the simulated outcomes, confirming the effectiveness of the FSS reflector-based antenna for V2V communication in IoT applications.

Keywords

V2V, Communication, IoT, Gain Enhancement, FSS, Reflector, Fabrication, Validation

1. Introduction

Research on the Internet of Vehicles (IOV) [1], including vehicle-to-everything (V2X), vehicle-to-vehicle (V2V), vehicle-to-network (V2N), and vehicle-to-information (IVI) communication, has flourished [2, 3] as a result of the continuous increase in demand for antennas for use in automotive communication systems. Through the connection of the Internet of vehicles and the base station, the Intelligent Transportation System (ITS) will be able to obtain real-time traffic information in the future, including information about pedestrians, road conditions, and information about roads. This information will also help to improve driving safety, prevent traffic jams, and increase the efficiency of transportation [4]. Moreover, cars are becoming a more integral part of our lives and are used by people to get to their destinations more and more frequently. The development of intelligent vehicle technology is a result of the above-mentioned reasons why increasing road traffic safety is a crucial concern [5]. The swift advancement of new technology and the Internet of Vehicles (IOV) have greatly facilitated our lives and transportation. Along with enhancing road safety, it has assisted governments in numerous nations and areas in efficiently managing the use of roads and highways. Additionally, V2X and satellite communication antennas in the ITS have drawn a lot of attention as vehicle communication technology has advanced [6].

Every car has a satellite link in addition to a V2V connection with adjacent vehicles and roadside units (RSUs) [7]. The main technologies of the existing vehicle communication system advance research on LEO satellite antennas for vehicle-to-vehicle connections [8, 9]. Apart from ensuring enhanced

WAISS'2024: 1st Euro-Mediterranean Workshop on Artificial Intelligence and Smart Systems, October 15, 2024, Djerba, Tunisia (Co-located with the 17th International Conference on Verification and Evaluation of Computer and Communication Systems (VECoS'2024), October 15-18, 2024, Djerba, Tunisia)

*Corresponding author.

ikram.troudi@isimg.tn (I. Troudi); chokri.baccouch13@gmail.com (C. Baccouch); mohamedali.boujemaa@supcom.tn (M. Boujemaa); abouahmed17@gmail.com (B. Chibani)

0009-0002-2107-4917 (I. Troudi); 0000-0003-3224-9911 (C. Baccouch); 0000-0002-9503-1699 (M. Boujemaa); 0000-0001-8631-6193 (B. Chibani)

safety during driving, like vehicle distance and remote driving, the V2X communication system further encompasses vehicle-to-infrastructure (V2I) connections. In order to predict the safest driving conditions and the shortest route to a destination, it offers numerous advanced features, including blind spot detection, emergency vehicle approach warning, forward distance warning, and road condition data. However, for these features to function properly, a high-performance antenna is necessary [10, 11].

Furthermore, due to the antenna's limited area of usage, building antennas for specific substrates like car windows or windshields is also difficult. Because of this, only extremely thin conductive strips can be utilized, which adds to the complexity of the antenna's design and installation [15]. Whatever the wireless communication product, antenna design ought to be given high importance. As a result, antenna engineers need to have a clear vision when making design selections. This includes considering factors like cost, area, and future achievability. There will be a high need for wireless data mass transit in the future. Antennas occupy a bigger space for communication between vehicles and low-orbit satellites than integrated circuits for data processing and analysis due to the coexistence of many wireless network broadcasts. In order to be more affordable and practical for today's multi-band wireless communication systems, the designed antenna must be small, multifunctional, and multi-band [16].

Many antennas used in LEO communication applications are constructed with multi-band and broadband in mind, in order to increase the diversity of the operational frequency of the antenna. These innovations include the use of tapered-angle power dividers and patch antennas. A dual-band effect can be achieved by increasing the bandwidth by 109% while maintaining a 2 dBi reduction in overall gain [10]. Bending the monopole antenna and adding branches has allowed for multi-band use. Multi-band use has been accomplished by increasing the dual-band bandwidth by 31.22% and 65.29% with a progressive adjustment in impedance [13]. Broadband can be achieved with a loop patch antenna design that uses partially slotted ground planes and rectangular slots. Enhancing antenna performance is the primary objective of employing parasitic loop elements [17]. In this design, the surface current at the operating frequency between the patch antenna elements is efficiently blocked or absorbed through the elliptical patch, the grounding branch, and the T-shaped branch, decreasing the mutual influence and creating a broadband effect [18]. The antenna can generate resonance at different frequencies by merging two bow-tie-like curves, which secures the multi-frequency effect. The antenna operates at a lower frequency due to the prolonged twists and turns [19].

A coplanar waveguide (CPW) structure X-band patch antenna that can be directly attached to the antenna and transmit receiver modules without the need for extra wire is suggested. As a result, unneeded movement can be stopped and antenna performance degradation can be minimized when external causes interfere [20]. Impedance bandwidth can also be obtained using rectangular slot patches by stacking perforated cylinders and etching a rectangular slot on the ground side. An antenna that combines the operating frequencies is called a broadband hybrid dielectric resonator antenna. As an alternative, the same aperture can be utilized on two frequency bands by combining array design with shared aperture technology [21, 22]. In patch antennas, the necessary radiation is produced by shorting pins and slots, which are cut into the surface to create resonance [23]. The rectangular microstrip patch can be truncated to produce broadband characteristics, and the electromagnetic bandgap structure can be used to produce notch features [24]. Loss can be decreased by the coplanar waveguide structure. Broadband can be achieved with a patch antenna and a wide impedance bandwidth by optimizing the radiation patch and the ground plane [25]. Broadband performance can be achieved with a defective ground structure (DGS) and a rectangular microstrip antenna. The antenna is 60×60 mm^2 in total [26]. In order to create a patch that is distinct from the conventional rectangle, they employ patch antennas and modify the structure. The broadband effect is achieved by using an elliptical radiator design. Reconfigurable circular polarization can be used to achieve 10.8–11.8 GHz and 14–15.4 GHz in dual-frequency bands for satellite communication applications, with bandwidths of 7.6% and 4.3%, respectively [27]. The entire antenna is built using substrate-integrated waveguides (SIWs), which result in a 9.85 GHz mixed-mode resonance. Dual resonances at 14 GHz result from cutting the short slit into the top of the cavity. Peak gains of 6.62 dBi and 6.44 dBi, respectively, were recorded by the antenna at 9.85 GHz and 14 GHz [28].

The document's remaining sections are organized as follows: The design and simulations of the

antenna element are shown in Section II, along with a discussion of the proposed FSS unit cell's geometry. In Section III, the antenna's simulation results with and without the FSS are evaluated. A 4×4 periodic design of the FSS is employed as a reflector to boost gain. The part also contains the measurement results to support the simulated outcomes. Lastly, the paper's closing observations are given in Section IV.

2. Antenna Geometry Design

2.1. Design of Microstrip Antenna

The proposed microstrip antenna design is illustrated in Figure 1. The antenna dimensions were carefully optimized using CST Microwave Studio's parametric sweep function to achieve the desired resonance at 5.9 GHz while maintaining a compact size.

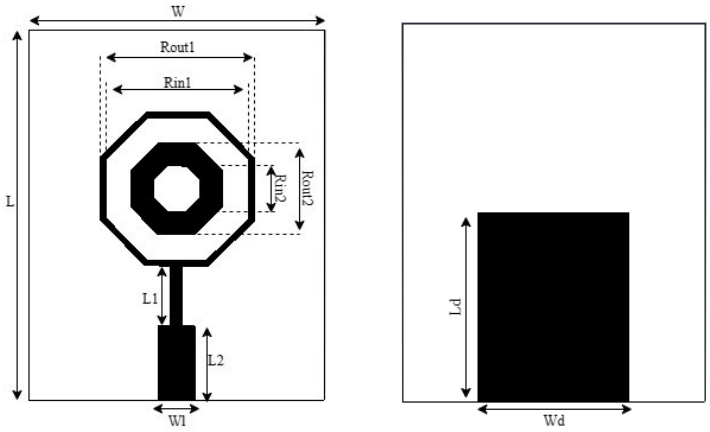

Figure 1: Top and bottom views of the proposed microstrip antenna.

The length (L) is 30 mm, and the width (W) is 24 mm. The substrate thickness (h) is 1.6 mm. An FR4 substrate with a relative permittivity of $\varepsilon_r = 4.3$ and a loss tangent of 0.025 was chosen for its cost-effectiveness and availability as shown in Tabe 1.

Dimensions of the proposed microstrip antenna.

Parameter	Value (mm)
L	30
W	24
R_{out1}	13
R_{in1}	12.5
R_{out2}	4
R_{in2}	2
W_l	3
L_1	5
L_2	6
L_d	15
W_d	12
h	1.6
t	0.035

Based on the proposed microstrip antenna, Figure 2 shows how the reflection parameter S11 varies with frequency.

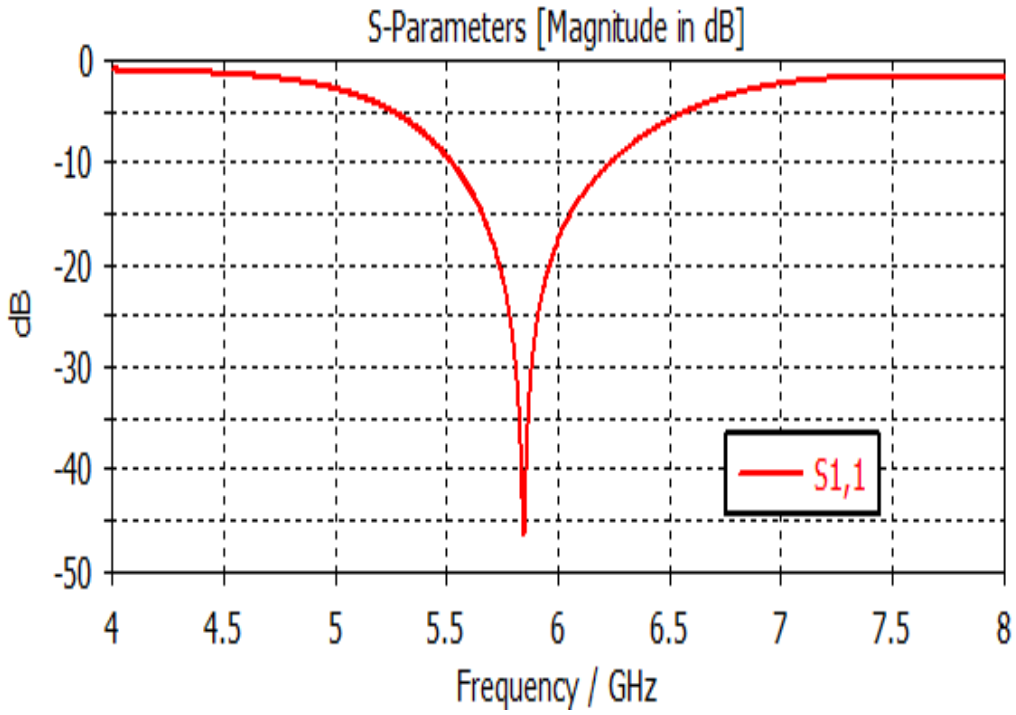

Figure 2: Reflection Coefficient of the proposed microstrip antenna

2.2. Design of Frequency Selective Surface Proposed

Figure 3 presents the dimensions of the proposed Frequency Selective Surface (FSS) decagonal unit cell, which were optimized through parametric studies using CST Microwave Studio. This novel layout functions as a reflector, guiding electromagnetic waves toward a main lobe of operation.

The FSS structure is fabricated on an FR-4 substrate with a thickness of 1.6 mm, a dielectric constant of $\varepsilon_r = 4.3$, and a loss tangent of 0.025. The unit cell consists of two concentric decagons, with outer and inner diameters $D_1 = 6.8$ mm and $D_2 = 5.8$ mm, respectively. The total surface area of each unit cell is $15\ \text{mm} \times 15\ \text{mm}$.

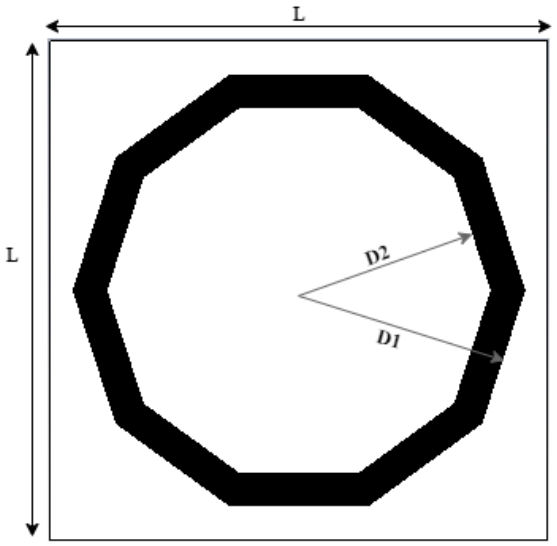

Figure 3: Geometry of the proposed decagonal FSS unit cell.

Figure 4 compares the reflection coefficients (S_{11}) of the antenna with and without the FSS reflector. The inclusion of the FSS significantly improves the antenna's impedance matching and overall performance. Specifically, the S_{11} value is reduced from -25.16 dB to -46.34 dB at the operating frequency of 5.9 GHz. This substantial reduction indicates enhanced energy transfer and reduced reflection.

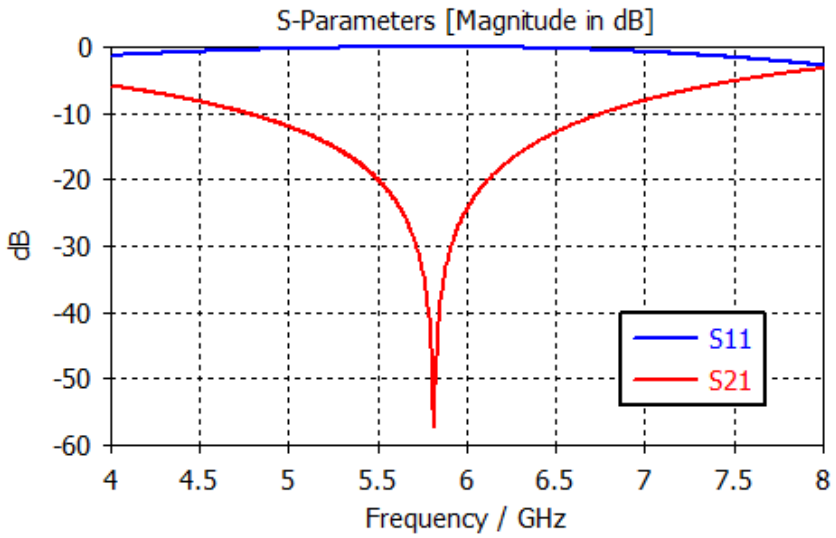

Figure 4: Simulated reflection coefficient S_{11} and transmission coefficient S_{21} of the antenna with and without FSS reflector.

Furthermore, the antenna exhibits a -10 dB bandwidth of 738.86 MHz centered around 5.9 GHz. This bandwidth is well-suited for V2V communication operating within the Dedicated Short Range Communication (DSRC) system band, making the design effective for vehicular communication applications. The Frequency Selective Surface (FSS) is structured as a 4×4 grid of unit cells. Each cell measures $60\ \text{mm} \times 60\ \text{mm}$ and is arranged with a periodicity of $2\ \text{mm}$. The dimensions of the unit cells are consistent with those of the overall array, ensuring uniform electromagnetic behavior and facilitating constructive interference in the desired frequency band.

3. Result and Discussion

3.1. Result with CST

In this section, a thorough analysis is conducted on the antenna's reflection coefficients, gain, and radiation pattern within the context of IoT communication. The arrangement of a Frequency Selective Surface (FSS) array positioned behind the antenna is illustrated in Figure 5. It is observed that the optimal reflection occurs when the distance between the antenna and the FSS array is equal to the wavelength λ corresponding to the resonant frequency of 5.9 GHz.

The concept of constructive interference plays a key role in enhancing antenna performance. The phase difference between the direct and reflected waves is calculated using the equation:

$$\varphi = 2\pi \left(\frac{2d}{\lambda} \right) + \pi$$

where d represents the distance between the antenna and the FSS, and λ is the wavelength. When the distance is set to $d = \frac{3\lambda}{4}$, the phase difference becomes:

$$\varphi = 2\pi \left(\frac{2 \cdot 3\lambda/4}{\lambda} \right) + \pi = 4\pi$$

A phase difference of 4π (or any multiple of 2π) ensures that the direct and reflected waves are in phase, resulting in constructive interference. This phenomenon leads to an increase in the overall gain of the antenna.

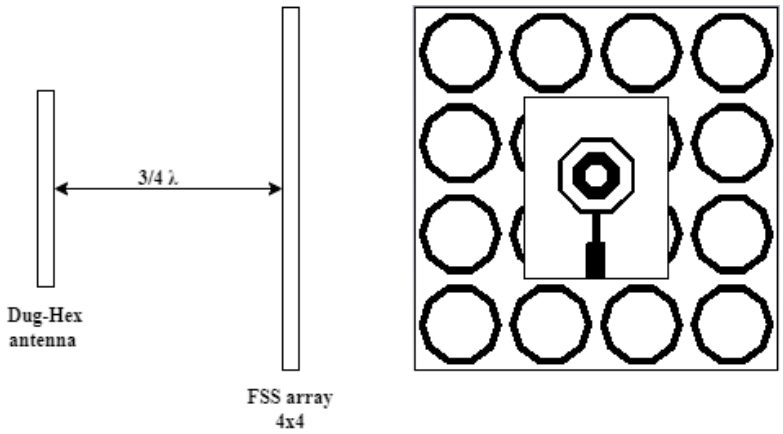

Figure 5: Side profile of the Dug-Hex antenna with FSS reflector.

To facilitate this constructive interference, the antenna emits a wave that propagates upward from the patch and downward through the partial ground plane. By introducing a reflector composed of FSS cells at a distance of λ from the antenna, the downward wave is redirected back toward the patch, acting as an additional source of radiation. The antenna then combines two waves: the primary wave emitted from the patch and the secondary wave reflected by the FSS. Since these waves are in phase, they interfere constructively, modifying the radiation pattern and enhancing both directivity and gain.

Furthermore, when integrated into an electronic circuit, the antenna serves as an effective electromagnetic shield for the ground plane. This integration significantly contributes to the antenna's functionality in facilitating Internet of Things (IoT) communication, thereby enhancing its utility in modern applications.

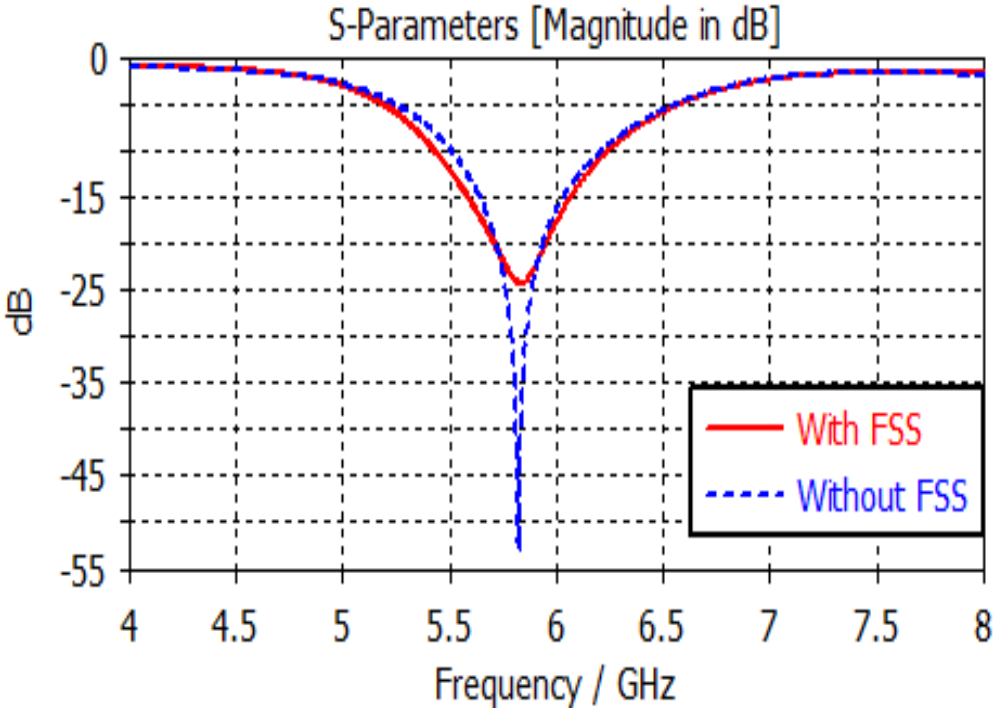

Figure 6: Reflection coefficient S_{11} of the patch antenna without and with FSS reflector.

The reflection coefficient (S_{11}) of the antenna is significantly influenced by the presence of the FSS, as illustrated in Figure 6. The graph shows a substantial decrease in the input reflection coefficient value, from -25.16 dB to -46.34 dB at the operating frequency of 5.9 GHz. Additionally, the antenna's

-10 dB bandwidth, centered at 5.9 GHz, is measured at 738.86 MHz. This bandwidth is suitable for Vehicle-to-Vehicle (V2V) communication within the Dedicated Short Range Communication (DSRC) frequency band. The comparison highlights the improved impedance matching and bandwidth enhancement achieved through FSS integration.

As shown in Figure 7, the gain of the antenna is significantly enhanced when the FSS reflector is employed. The peak gain increases from 1.46 dB to 6.42 dB at 5.9 GHz. This enhancement occurs without altering the antenna's geometry or materials, demonstrating the efficiency of using a passive FSS structure to improve radiation performance.

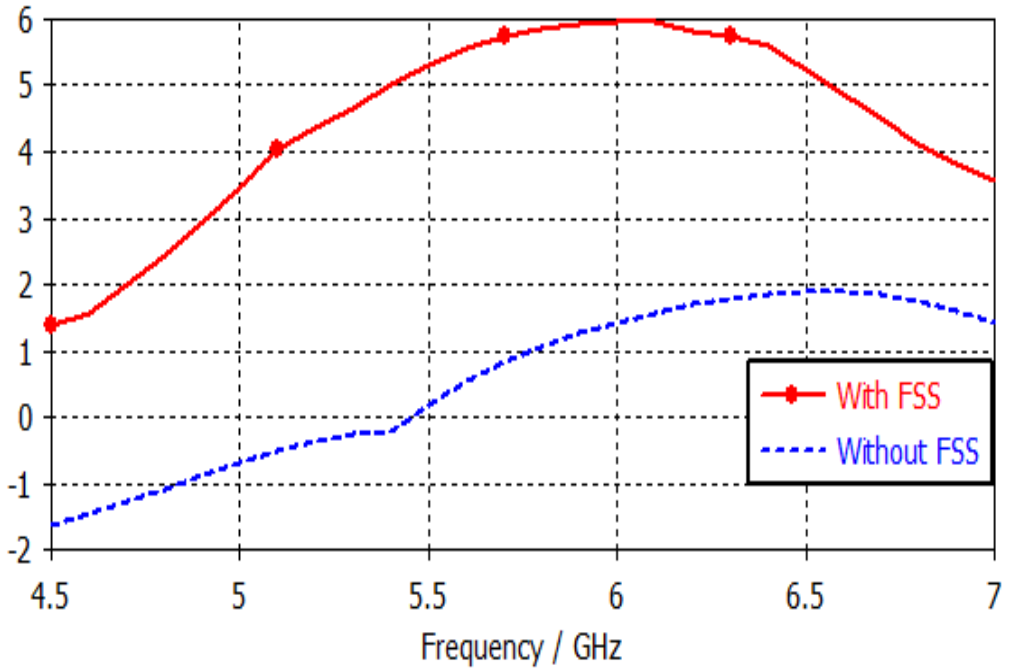

Figure 7: Antenna gain evaluation with and without FSS reflector.

Figure 8 compares the far-field radiation patterns in the E-plane ($\phi = 0°$) and H-plane ($\phi = 90°$) at 5.9 GHz. Although the general shape of the patterns remains stable with or without FSS, notable modifications in lobe structure and directionality are observed. These variations confirm that the integration of FSS modifies the electromagnetic behavior of the antenna, leading to improved directional performance and reduced back radiation.

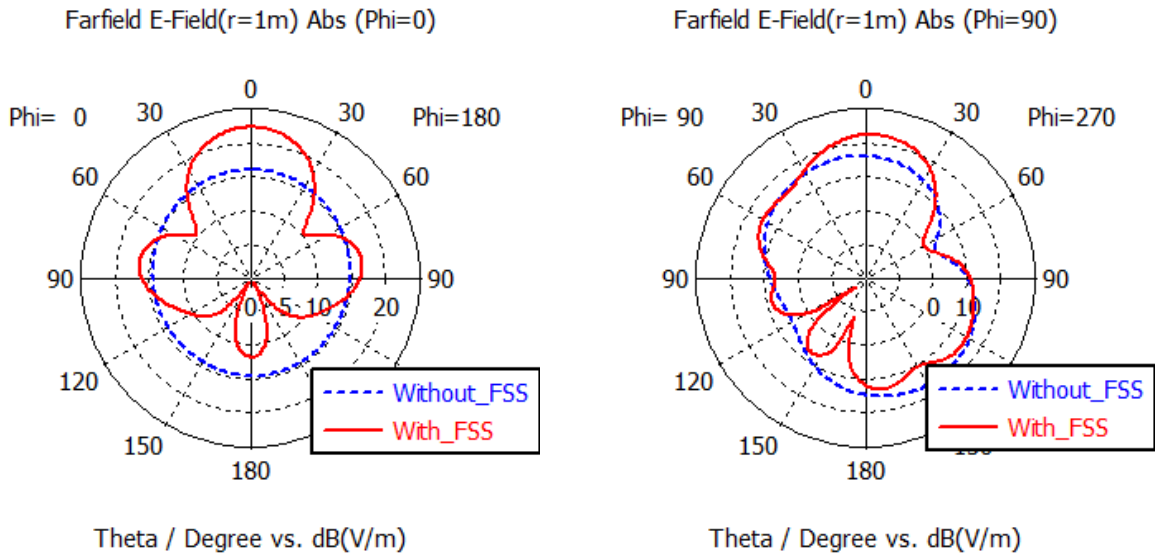

(a)

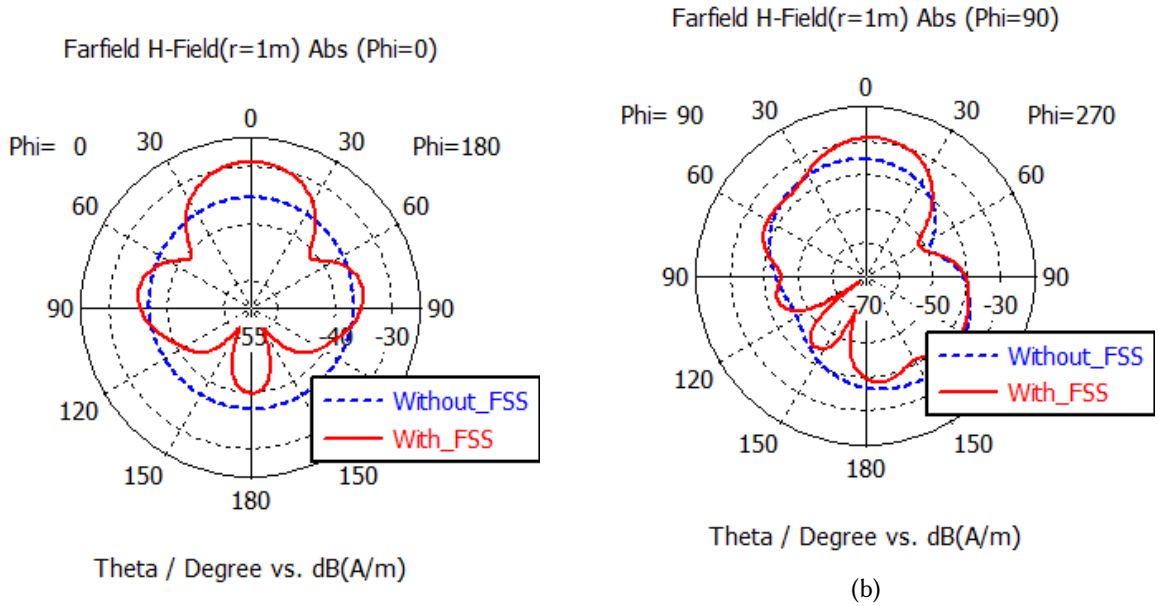

(b)

Figure 8: Simulated radiation patterns of the antenna with and without FSS at 5.9 GHz: (a) E-plane, (b) H-plane.

Figure 9 demonstrates that the antenna achieves an efficiency exceeding 87.45% within the operating frequency band. This high efficiency validates the suitability of the proposed structure for IoT applications requiring reliable and energy-efficient wireless links.

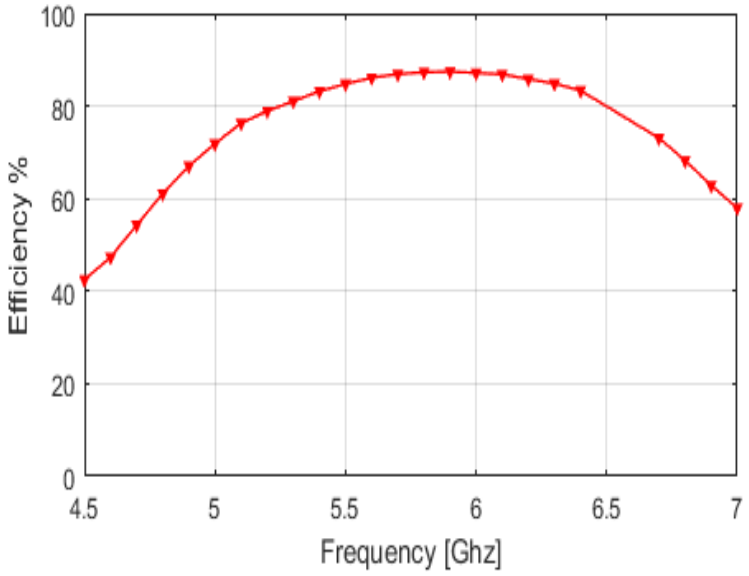

Figure 9: Efficiency of the patch antenna as a function of frequency with FSS integration.

As illustrated in Figure 10, the Voltage Standing Wave Ratio (VSWR) at 5.9 GHz is approximately 1.17, well below the threshold value of 2. This indicates excellent impedance matching between the feed line and the antenna, ensuring maximum power transfer and minimal reflection loss.

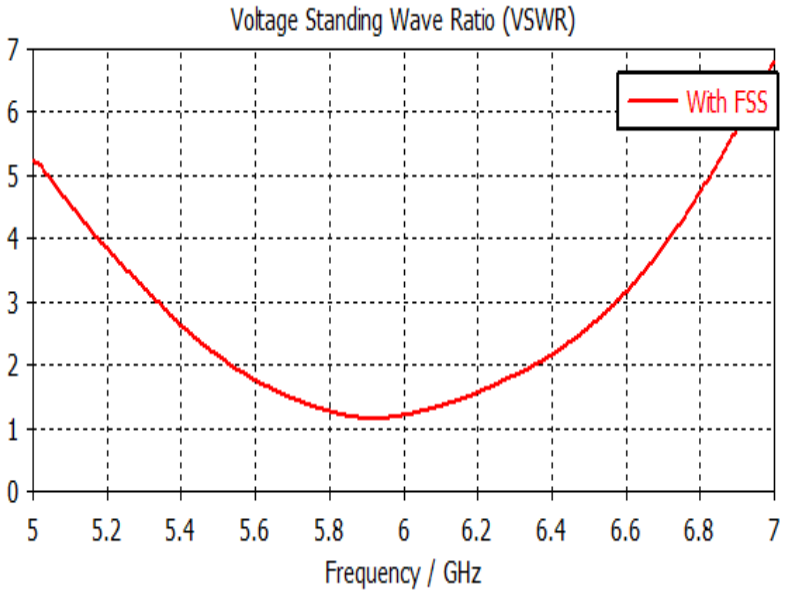

Figure 10: Voltage Standing Wave Ratio (VSWR) of the antenna with FSS at 5.9 GHz.

3.2. Validation of the Result

To experimentally validate the proposed Dug-Hex antenna and FSS design, a fabrication process was carried out in a fabrication laboratory, as illustrated in Figures 11 and 12.

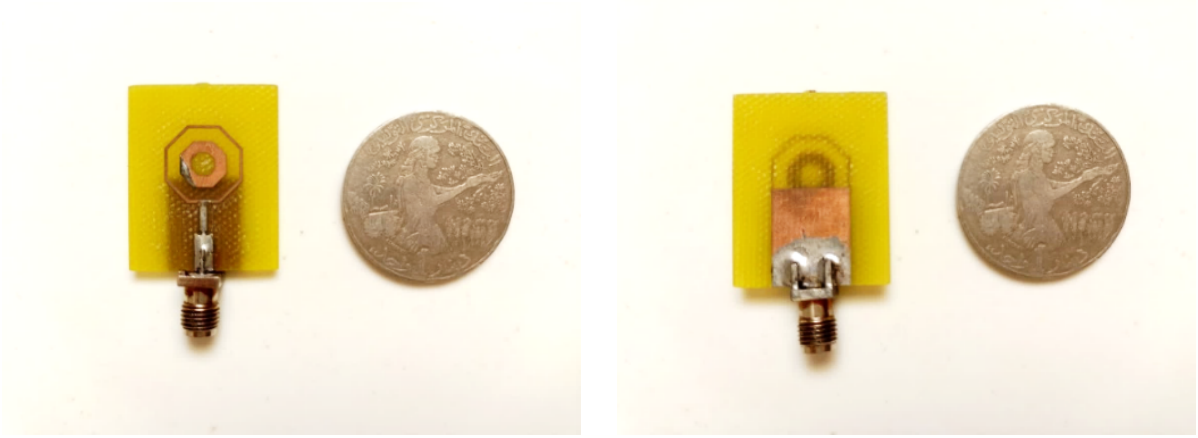

(a) (b)

Figure 11: Fabricated Design Dug-hex antenna proposed.

The fabrication followed the parameters listed previously, using FR-4 substrate and copper metallization, consistent with the CST simulation setup. Standard printed circuit board (PCB) manufacturing techniques were employed to realize the prototype.

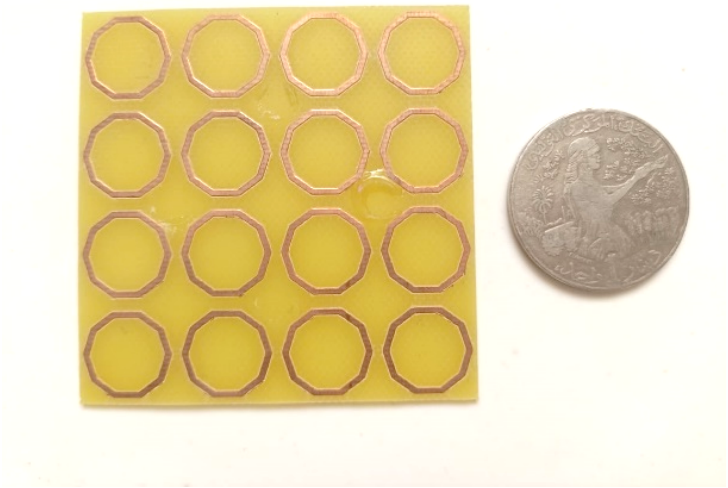

Figure 12: Fabricated structure of the proposed Frequency Selective Surface (FSS).

Figure 13 shows no significant difference between the measured and simulated S-parameters for both configurations, with and without the FSS. Both sets of results align closely, indicating that the experimental data matches the theoretical predictions. This confirms the accuracy of the design and fabrication process, validating the performance of the proposed dug-hex antenna and FSS.

As observed in Figure 13, the measured results show excellent agreement with the simulations for both configurations. The close alignment of the S_{11} responses confirms the reliability of the design process and validates the performance enhancement achieved through FSS integration. These results demonstrate that the proposed structure is both practically realizable and effective for IoT and V2V communication applications.

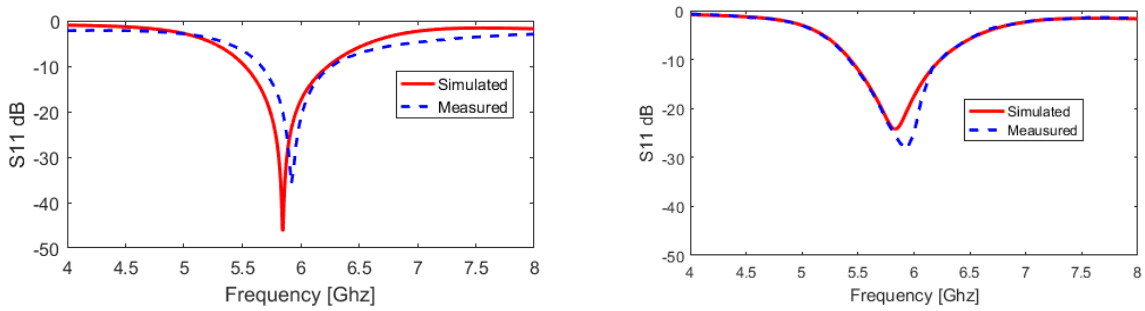

Figure 13: Measured and simulated S_{11} parameters of the antenna: (a) without FSS, (b) with FSS.

4. Conclusion

This study has demonstrated the effectiveness of integrating a Frequency Selective Surface (FSS) reflector with a compact antenna structure to enhance performance for Vehicle-to-Vehicle (V2V) communication in Internet of Things (IoT) environments. The proposed design achieved a significant gain improvement from 1.46 dB to 6.42 dB at 5.9 GHz, along with a broadened bandwidth of 738.86 MHz. These enhancements were achieved without negatively affecting the antenna's transmission characteristics.

To validate the proposed architecture, a prototype was fabricated using standard PCB manufacturing techniques. The measured results closely aligned with simulation outcomes, thereby confirming the reliability and feasibility of the design.

The findings highlight the strong potential of FSS-based reflectors for improving gain and bandwidth in V2V and IoT applications. Future work may involve further optimization of the FSS geometry, as well as exploring hybrid or adaptive structures for multi-band or reconfigurable antenna systems targeted toward next-generation vehicular communication networks.

Declaration on Generative AI

The authors have not employed any Generative AI tools.

References

[1] Khalifa, M. O., Yacoub, A. M., & Aloi, D. N. (2021). A multiwideband compact antenna design for vehicular sub-6 GHz 5G wireless systems. *IEEE Transactions on Antennas and Propagation*, 69(12), 8136–8142.

[2] Kumar, G., & Mikkili, S. (2023). Critical review of vehicle-to-everything (V2X) topologies: Communication, power flow characteristics, challenges, and opportunities. *CPSS Transactions on Power Electronics and Applications*.

[3] Khalid, S., et al. (2023). Optimising Video Transmission Performance in 5G New Radio Technology for Vehicle-to-Network (V2N) Application: A Comprehensive Analysis. In *Proc. 11th Int. Conf. on Information and Communication Technology (ICoICT)*, IEEE.

[4] Wang, R., et al. (2020). Low-profile implementation of U-shaped power quasi-isotropic antennas for intra-vehicle wireless communications. *IEEE Access*, 8, 48557–48565.

[5] Michel, A., Singh, R. K., & Nepa, P. (2022). A compact and wideband dashboard antenna for vehicular LTE/5G wireless communications. *Electronics*, 11(13), 1923.

[6] Yang, P., Yang, R., & Li, Y. (2021). Dual circularly polarized split beam generation by a metasurface sandwich-based Fabry–Pérot resonator antenna in Ku-band. *IEEE Antennas and Wireless Propagation Letters*, 20(6), 933–937.

[7] Wang, W., & Zheng, Y. (2021). Wideband gain enhancement of a dual-polarized MIMO vehicular antenna. *IEEE Transactions on Vehicular Technology*, 70(8), 7897–7907.
[8] Pirapaharan, K., et al. (2022). Smart, Fast, and Low Memory Beam-Steering Antenna Configurations for 5G and Future Wireless Systems. *Electronics*, 11(17), 2658.
[9] Kraus, D., et al. (2022). Towards a recommender system for in-vehicle antenna placement in harsh propagation environments. *Sensors*, 22(17), 6339.
[10] Bryant, B., et al. (2022). Design of Triple-Band (DSRC, 5G, 6G) Antenna for Autonomous Vehicle Telematics. *Electronics*, 11, 2523.
[11] Im, C., et al. (2021). Design of a printed 5G monopole antenna on vehicle window glass using parasitic elements and a lattice-structure reflector for gain enhancement. *Applied Sciences*, 11(21), 9953.
[12] Kumar, R., & Arnon, S. (2022). SNR optimization for LEO satellite at sub-THz frequencies. *IEEE Transactions on Antennas and Propagation*, 70(6), 4449–4458.
[13] Chung, M.-A., & Yang, C.-W. (2021). Miniaturized broadband-multiband planar monopole antenna in autonomous vehicles communication system device. *Electronics*, 10(21), 2715.
[14] Chung, M.-A., & Yang, C.-W. (2021). A miniaturized planar monopole antenna based on a coupling structure for compact mobile IoT and EVs device applications. *International Journal of Antennas and Propagation*, Article ID 7535382.
[15] Liu, X., et al. (2020). Integrated frequency selective surface and antenna printed on a transparent substrate. *IEEE Antennas and Wireless Propagation Letters*, 19(12), 2062–2066.
[16] Wang, W., et al. (2021). Compact dual-polarized wideband antenna with dual-/single-band shifting for microbase station applications. *IEEE Transactions on Antennas and Propagation*, 69(11), 7323–7332.
[17] Hossain, A., et al. (2020). An octagonal ring-shaped parasitic resonator based compact ultrawideband antenna for microwave imaging applications. *Sensors*, 20(5), 1354.
[18] Mu, W., et al. (2022). A flower-shaped miniaturized UWB-MIMO antenna with high isolation. *Electronics*, 11(14), 2190.
[19] Chletsou, A., Locke, J. F., & Papapolymerou, J. (2021). Vehicle platform effects on flexible, lightweight, and dual-band antenna performance. *IEEE Journal of Microwaves*, 2(1), 123–133.
[20] Jang, D., et al. (2022). Design of a high-durability X-band patch antenna with CPW feeding based on durability evaluation. *Electronics*, 11(4), 553.
[21] Zubir, I. A., et al. (2020). A low-profile hybrid multi-permittivity dielectric resonator antenna with perforated structure for Ku and K bands. *IEEE Access*, 8, 151219–151228.
[22] Abdollahvand, M., et al. (2020). A 20/30 GHz reflectarray backed by FSS for shared aperture Ku/Ka-band satellite antennas. *IEEE Antennas and Wireless Propagation Letters*, 19(4), 566–570.
[23] Liang, T., Wang, Z., & Dong, Y. (2020). A circularly polarized SIW slot antenna based on high-order dual-mode cavity. *IEEE Antennas and Wireless Propagation Letters*, 19(3), 388–392.
[24] Abbas, A., et al. (2020). A rectangular notch-band UWB antenna with controllable notched bandwidth and center frequency. *Sensors*, 20(3), 777.
[25] Agarwal, S., et al. (2021). Double Overt-Leaf Shaped CPW-Fed Four Port UWB MIMO Antenna. *Electronics*, 10, 3140.
[26] Sarkar, T., et al. (2019). DGS-integrated air-loaded wideband microstrip antenna for X- and Ku-band. *IEEE Antennas and Wireless Propagation Letters*, 19(1), 114–118.
[27] Baladi, E., et al. (2021). Dual-band circularly polarized fully reconfigurable reflectarray antenna for satellite applications in the Ku-band. *IEEE Transactions on Antennas and Propagation*, 69(12), 8387–8396.
[28] Lokeshwar, B., Venkatasekhar, D., & Sudhakar, A. (2020). Dual-band low-profile SIW cavity-backed antenna using bilateral slots. *Progress In Electromagnetics Research C*, 100, 263–273.